

# Measurement-Based Optimization of Thermal Networks for Temperature Monitoring of Outer Rotor PM Machines

Daniel Wöckinger\*, Gerd Bramerdorfer\*, Senior Member, IEEE, Stephan Drexler\*,  
Silvio Vaschetto<sup>§</sup>, Senior Member, IEEE, Andrea Cavagnino<sup>§</sup>, Fellow, IEEE,  
Alberto Tenconi<sup>§</sup>, Senior Member, IEEE, Wolfgang Amrhein\*, and Frank Jeske<sup>†</sup>

\* Department of Electrical Drives and Power Electronics, Johannes Kepler University Linz, Linz, Austria

<sup>§</sup> Dipartimento Energia, Politecnico di Torino, Turin, Italy

<sup>†</sup> Ebm-papst St. Georgen GmbH & Co. KG, St. Georgen, Germany

Email: daniel.woeckinger@jku.at

**Abstract**—This paper is about deriving suitable lumped parameter thermal networks for modeling the transient thermal characteristics of electric machines under variable load conditions. The network should allow for an accurate estimation of the temperatures of critical machines' components. In best case, the model can be run in real time to adapt the motor control based on the load history and maximum permissible temperatures. Consequently, the machine's capabilities can be exhausted at best considering a highly-utilized drive. The model further shall be as simple as possible while guaranteeing a decent accuracy of the predicted temperatures. A lumped parameter thermal network is selected and its characteristics are explained in detail. Besides the model selection and the optimization of its critical parameters through an evolutionary optimization strategy, an experimental setup will be described in detail. The model accuracy is evaluated for both static and dynamic test cycles with changing load torque and speed requirements. Finally, the significant improvement of the accuracy of the predicted motor temperatures is presented and the results are compared with measurements.

**Index Terms**—electric machines, evolutionary algorithm, lumped parameter thermal network, optimization, outer rotor, permanent magnet synchronous machine

## I. INTRODUCTION

Nowadays, electric machines are particularly optimized for any individual application. The variety of optimization scenarios is manifold, as different machine types, problem definitions, and methods for solving those problems are considered [1]–[4]. In the past, most of the optimization scenarios focused on the electromagnetic analysis while other domains, e.g., the thermal or mechanical characteristics, where neglected or only a rough estimate was considered. Now, evermore researchers focus on a multiphysics-based approach, such as in [5], [6]. Besides, a system-level approach is frequently considered to capture the interaction of electric machine, power electronics, and control aspects [7]. To allow for fast evaluation of thermal characteristics, usually the modeling is focused on most important temperatures and heat flow paths. Research is also done to minimize the thermal models' complexity while guaranteeing acceptable accuracy [8]. In terms of thermal

modeling, different approaches were followed in the past. They can be categorized as follows:

- 1) Expert knowledge based thermal modeling
- 2) Thermal modeling based on artificial intelligence techniques
- 3) A combination of (1) and (2)

Category (1) consists of modeling approaches where the model structure and respective coefficients, parameters, etc. are solely determined based on expert knowledge regarding the physical circumstances. Besides computing the quantities based on machines' dimensions and materials' properties, auxiliary measurements used for calibration are sometimes taken into account. Nevertheless, the applied modeling techniques are always developed based on fundamentals from engineering science. Some examples can be found in [9]–[13].

Category (2) refers to approaches where the modeling is done without taking into account the physical circumstances in detail. In [14]–[17] recent activities are presented. Such approaches allow for a higher feasibility in the model definition. For instance, by contrast to the first category, an indirect modeling of the temperatures, e.g., with regard to the machine's torque and speed, can be accomplished. Thus, no direct physical relation of modeling input and output must be available. The derived models are often of black-box type, which can be unfavorable. As an example, there is no possibility for obtaining particular machine-specific information to gain insights. Thus, while for group (1), similar machines can be modeled with limited additional effort, for group (2) usually all the modeling efforts have to be again started from scratch. Besides, it is very hard or even impossible to proof general stability of black-box models.

Category (3): this category finally embraces approaches where both, physical expertise, as well as new techniques from mathematics regarding modeling and optimization are taken into account. Some examples can be found in [18], [19].

Obviously, there are fluid boundaries among the categories.



Fig. 1: Motor under test.

Outer rotor SPM	
Number of phases	3 $\Delta$
Number of pole pairs	2
Phase connection	$\Delta$
Rated DC bus voltage	24 V
Rated DC bus current	5.1 A
Rated speed	7100 rpm
Rated torque	150 mNm
Terminal resistance (at 20 °C)	0.427 $\Omega$

TABLE I: Characteristic motor data.

Throughout this work, the authors focus on category (3). A lumped parameter thermal network (LPTN) is selected based on expert knowledge for the outer rotor surface permanent magnet (SPM) machine under test. Afterwards, an optimization of critical parameters of the network is done using an evolutionary algorithm. In order to minimize the runtime, the design space regarding the thermal parameters of the optimization problem is constrained based on expert knowledge. The data for model verification are obtained through measurements conducted by using an experimental setup.

The following content is organized as follows: in the next Section II the motor under test is introduced. Section III presents the selected LPTN and discusses critical parameters and the residual settings of the model. Consequently, Section IV is about the experimental setup used for this work. Sample data obtained by measurements are presented for all considered machine components. Finally, expert-based calibration and optimization of parameters that are difficult to predict are presented in Section V. This is completed by a detailed comparison of modeling results versus additional measurements. Finally, a summary and an outlook about future activities is illustrated in Section VI.

## II. MOTOR UNDER TEST

In this paper, the thermal characteristics of a 3-phase, brushless SPM machine with outer rotor topology is studied.

The motor with disassembled rotor is shown in Fig.1. It has a rated power of 110 W at 150 mNm and 7100 rpm. Its most important data, as well as its electrical characteristics are summarized in Table I. One big challenge of creating a thermal model for this type of machine is the rotating bell in the air that leads to a complex overall heat flux. Additionally, an air gap between rotor bell and mounting flange allows air- and heat-exchange, which makes modeling even more challenging.

## III. LUMPED PARAMETER THERMAL NETWORK

The lumped parameter thermal network selected to model the outer rotor SPM machine under test is depicted in Fig. 2. In detail, the cross section in Fig. 2a highlights the outer rotor bell structure that includes the rotor yoke and the permanent magnets, and the inner part of the machine that consists of the stator core and the windings, and the hollow stator fixture that connects the stator yoke to the mounting flange. The machine's shaft, which is connected to the rotor bell, rotates in the inner part of the air-filled stator fixture thanks to ball bearings. Considering the axisymmetric geometry of the machine, Fig. 2b depicts the five-node LPTN proposed for the thermal analysis of this outer rotor SPM machine. In detail, for a defined ambient temperature ( $T_a$ ), this thermal network allows evaluating the average temperatures for the rotor ( $T_r$ ), the air gap ( $T_{air}$ ), the stator winding ( $T_w$ ), the stator yoke ( $T_y$ ), and the stator fixture ( $T_f$ ).

The current sources represent the heat generators related to the machine losses, that are the stator Joule ( $P_{Js}$ ) and iron ( $P_{Fe}$ ) losses, and the entire rotor losses ( $P_{rot}$ ). In order to limit the number of nodes and the complexity of the network, all the loss components in the machine can be reasonably linked to one of this three heat sources that are considered as uniformly distributed within their particularly associated component. For example, in the conducted analysis  $P_{rot}$  includes the magnets' and the rotor back iron losses. Finally, the heat source  $P_{iron}$  combines the iron losses in the stator lamination and friction losses in the bearings.

The thermal resistances represent the different heat flow paths inside the machine and allow computing the steady-state temperatures, while the thermal capacitances allow modeling the thermal transient behavior. If the machine's geometrical dimensions and the material properties are known, these thermal parameters can be mainly computed using equations reported in literature [10]. In particular, the thermal capacitances of the stator teeth ( $C_{teeth}$ ), stator yoke ( $C_{sy}$ ), stator fixture ( $C_{sfy}$ ) and of the rotor bell plus magnets ( $C_{rot}$ ) can be easily obtained by the product of the component's weights and the specific heat capacity of their materials, while the thermal resistances are usually computed considering the different machine parts as hollow cylinders. It has to be highlighted that the complete machine does not have a symmetry with respect to the central plane of the stator. Therefore, the adoption of the hollow cylinder theory to simplify the thermal paths is a rough approximation. In addition, the studied machine features a pancake shape where the end effects may result in non-negligible axial heat paths that affect the heat flows in radial

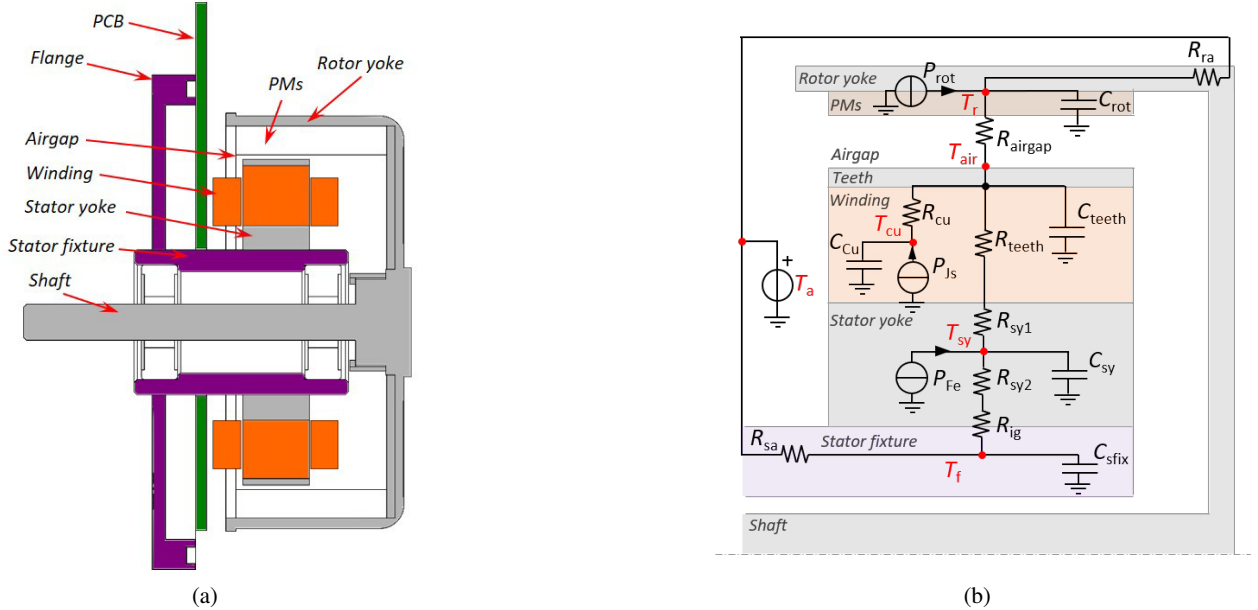


Fig. 2: Sketch of the cross section for the SPM outer rotor machine (a) and proposed lumped parameter thermal network (b).

direction. Nevertheless, the well-known hollow cylinder theory has been assumed as a simplified and practical approach for the initial set of the thermal network parameters.

Looking at Fig. 2b, the thermal resistances  $R_{teeth}$ ,  $R_{sy1}$  and  $R_{sy2}$  define the thermal flux across the teeth and the stator yoke. In particular, the stator yoke has been subdivided into two parts, such that the stator iron losses are considered impressed in the middle of the stator yoke. Through these elements, the heat transfer is due to conduction, and the thermal resistances can be easily computed by

$$R_{cond} = \frac{1}{2\pi k_{ir} L_s p_{ir}} \ln \left( \frac{r_{out}}{r_{in}} \right). \quad (1)$$

In (1),  $k_{ir}$  is the thermal conductivity coefficient of the iron,  $L_s$  is the core length, and  $r_{in}$  and  $r_{out}$  are the inner and outer radii of the hollow cylinder that represents the considered machine part. The coefficient  $p_{ir}$  is the volume ratio between the stator teeth iron and the total teeth plus slot volume; for the computation of  $R_{teeth}$  this coefficient is smaller than one, while for the yoke thermal resistance  $p_{ir}$  is equal to 1.

However, applying the knowledge of the geometrical or physical characteristics is not always straightforward for the LPTN parameters considered in Section III-A. For these parameters, reliable values can be obtained by means of accurate calibrations, based on DC tests or convection heat transfer and flow calculations [9], [10], [20]. The values of the computed or calibrated parameters of the assumed thermal network are listed in Table III.

#### A. Expert-based calibration of model parameters

The thermal resistance and capacitance of the stator winding cannot be easily computed because of the presence of air and non-uniformly distributed insulation layers between copper

and iron, including resins and enamels. However, an equivalent thermal resistance ( $R_{cu}$ ) and capacitance ( $C_{cu}$ ) between stator copper and stator iron can be obtained through a short-time DC thermal test according to the procedure described in [21]. Since the machine under test is delta connected, the test has been executed supplying the current in one stator phase with the other two connected in parallel to the first one.

Additionally, the determination of the air gap thermal resistance is not trivial. The heat exchange between stator and rotor through the air gap can either be due to convection or radiation phenomena. Nevertheless, in previous activities related to induction motors, the authors verified that for thin air gap the thermal exchange can be equivalently modeled as a conductive thermal path in stationary air [10]. Since the machine under test features a small air gap thickness (0.5 mm) and the magnets are ring-shaped, also in this case the initial value for the air gap thermal resistance has been conveniently computed by (1).

The heat exchange between the machine and external ambient is modeled through the thermal resistances  $R_{sa}$  and  $R_{ra}$ . Despite these parameters can be obtained by dedicated DC thermal tests as well, it is possible to approximate their values by analytical evaluations, as done by the authors for this research activity. In detail,  $R_{sa}$  models both the heat conduction along the stator fixture and the flange, as well as the convective heat exchange between the flange and the ambient. For the initial definition of the network parameters, the authors computed the conduction thermal resistance for the stator fixture indicated in Fig. 2a and opportunely increased this value in order to consider the presence of the flange.

The thermal resistance  $R_{ra}$  that represents the heat exchange between the rotor bell and the ambient assumes different values depending on whether the rotor is rotating or not. In

detail, for standstill conditions the heat flow is due to natural convection only, while during the rotation both natural and forced convection phenomena are present. The initial values for the network setup have been computed by the authors using well-known and proven empirical heat transfer correlations reported in literature [9], [20].

Regarding  $R_{ig}$ , it could be estimated by either approximating the equivalent length of the interface gaps between stator yoke and stator fixture or, again, by means of a dedicated DC test. For the considered machine the interface gap has been estimated to be approximately  $30\text{ }\mu\text{m}$ .

#### IV. EXPERIMENTAL SETUP AND MEASUREMENT DATA

In order to verify the analytically derived thermal model, a test setup featuring an accurate measurement of the machine's temperatures is essential. In general, the transient temperature characteristics depend on the dynamic load profile that the machine is exposed to. Consequently, the experimental setup shown in Fig. 3a was designed for both the operation of the machine at different load points by controlling speed and torque, and a simultaneous acquisition of different temperatures within the machine. Its main components include the device under test (A), a hysteresis brake to apply various load points (B), a sensor to acquire speed and torque (C), and the power electronics for DC/AC conversion featuring a controller (D) for facilitating a field-oriented control of the machine to adjust the load point operation. Table II summarizes the key figures of the utilized torque-speed sensor and hysteresis brake.

##### A. Selected positions for temperature monitoring

The transient temperatures of the individual motor components are determined with sensors at various positions of interest. The internal structure of the motor, as well as its back with an attached mounting flange are illustrated in Fig. 3b and 3c, respectively. For characterizing and monitoring the main thermal paths from different heat sources through the machine's components to the ambient, the following temperatures are acquired by thermal sensors:

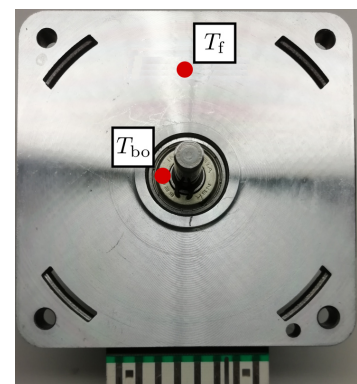
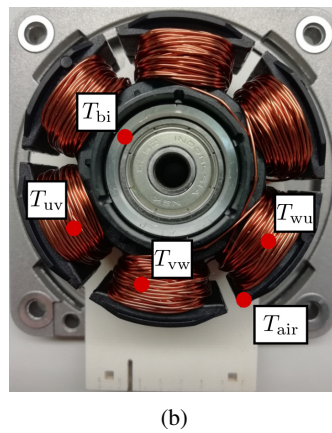
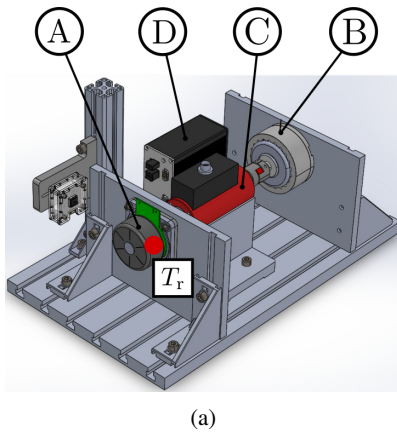


Fig. 3: (a) A CAD model of the test bench with the temperature measuring point  $T_r$ . (b) The stator front view and the considered temperature measuring points  $T_{uv}$ ,  $T_{vw}$ ,  $T_{wu}$ ,  $T_{bi}$ , and  $T_{air}$ . (c) The back plate view with the positions of  $T_f$  and  $T_{bo}$ .

Torque-speed sensor	
Maximum rupture torque	1 N m
Maximum speed	50 000 rpm
Torque measurement range	$\pm 200\text{ mNm}$
Output voltage	$\pm 5\text{ V}$
Hysteresis brake	
Rated current ( $I_n$ )	270 mA
Min. torque at $I_n$	1.2 Nm
Maximum kinetic power	110 W
Maximum speed $n_{\max}$	12 000 rpm
Drag torque at $n_{\max}$	7.77 mNm

TABLE II: Main specifications for the torque-speed sensor and the hysteresis brake used for the experimental measurements.

- $T_{uv}$ ,  $T_{vw}$ ,  $T_{wu}$  at the surface of one coil per phase;
- $T_{air}$  at the tip of one pole shoe of the stator yoke;
- $T_{bi}$  on the outer (static) ring of the inner ball bearing;
- $T_{bo}$  on the outer (static) ring of the outer ball bearing;
- $T_f$  on the mounting flange made of aluminum;
- $T_r$  on the outer side of the rotor.

Their spatial positions inside the motor are illustrated in Fig. 3. On the one hand, all temperatures except  $T_r$  can be measured with conventional thermocouples of type K, which are connected to the relevant surface by using a thermally conductive adhesive. Instead, the outer rotor temperature has to be measured by a contactless measuring method. For this purpose, a thermographic camera is used. Because of the given topology, the magnet's temperature cannot be directly measured.

##### B. Measurement results

In Fig. 4, sample data of one exemplary measurement cycle are presented. A stepwise random but reasonably bounded change of the load characterized by the respective torque and speed is considered. The transient characteristics of all eight

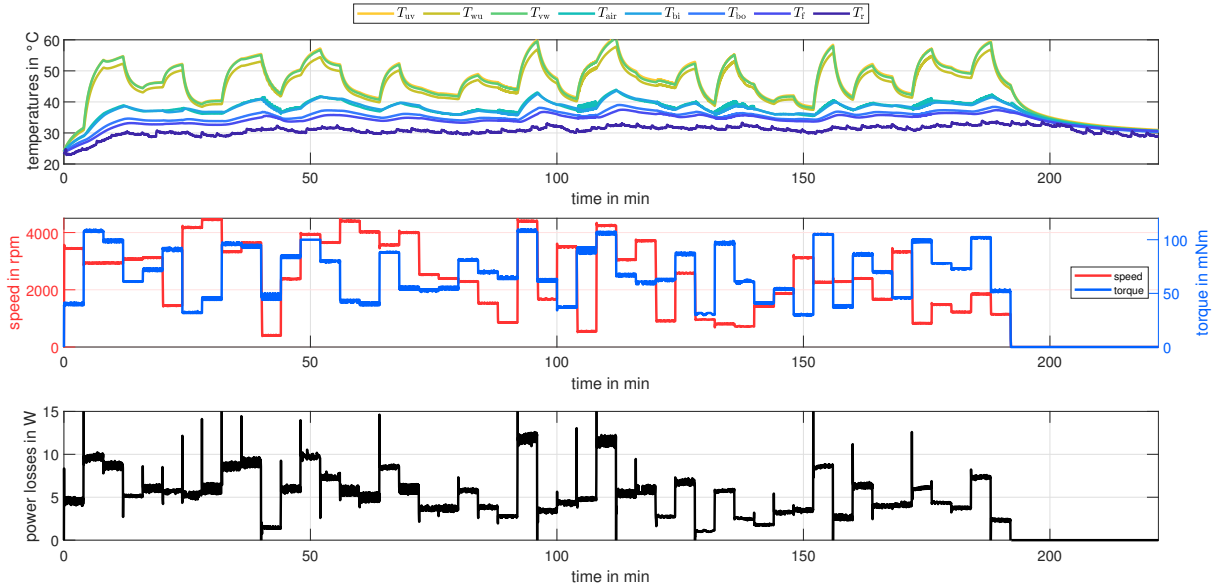


Fig. 4: A typical data set for transient load changes including the temperatures of all individual motor components, the speed and torque signals of applied load points, and the total power loss of the motor.

acquired temperatures are illustrated. As can be observed, the winding temperatures are highest followed by the stator lamination. This is due to the fact that the Joule losses are the major loss component, especially if the load torque is high. Because of the surrounding air inside the bell, the main heat flow applies from winding to the lamination. Nevertheless, at low load torques and high speeds, the amount of iron losses in the stator and the friction losses in the ball bearings cannot be neglected. For this reason, it would be a great simplification if the entire power losses are applied in the model at just one point, e.g. at the winding node through  $P_{js}$ , for the whole speed and torque range. In general, they are generated at different positions in the motor. As a result, a loss separation is discussed in the upcoming Section V-A, that subdivides the entire losses at different heat sources in the network.

Generally, the thermocouple-based measurements show negligible measurement noise. This is different for the rotor temperature  $T_r$ . However, it is based on measuring the temperature of a rotating cylindrical device. Thus, any manufacturing tolerance affecting the rotor's true running performance, as well as a slightly different temperature distribution along the rotor housing's outer perimeter might cause this effect. Additionally, the thermographic camera has an auto-calibration feature that leads to a peak in the data approximately every three minutes.

## V. PARAMETER OPTIMIZATION AND RESULTS

It was observed during modeling that the parameters  $R_{teeth}$ ,  $R_{sy1}$ ,  $R_{sy2}$ , and  $R_{ig}$ , that physically correspond to thermal conduction, can be determined with high accuracy based on expert knowledge. Furthermore, an individual weighting of all machine components and the manufacturer's information about their material properties allow a precise estimation of the heat

capacities  $C_{rot}$ ,  $C_{teeth}$ ,  $C_{ys}$ , and  $C_{sfix}$ . The parameters  $R_{cu}$  and  $C_{cu}$  are calibrated by separate measurements described in Section III that particularly focus on winding characteristic. By contrast, the quantities  $R_{airgap}$ ,  $R_{sa}$  and  $R_{ra}$  are sensitive to the exact machine's manufacturing and their heat transport phenomena are usually a combination of natural and forced convection, as well as heat conduction. Thus, in the following they are selected as optimization parameters. Nevertheless, the parameter range is constrained based on expert knowledge to avoid potentially accurate solutions that are meaningless from a physical point of view.

### A. Loss separation

As mentioned before, it is physically not correct to assign the entire amount of losses to the current source  $P_{js}$  in the network. For this reason, the measured total power losses  $P_{loss}$  presented in Fig. 4 have to be separated into Joule losses  $P_{js}$  associated with the ohmic resistance of the windings and residual losses  $P_{residual}$ . The latter includes mechanical power

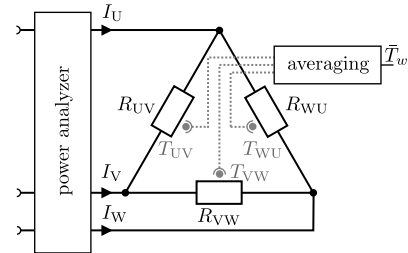


Fig. 5: Necessary measurements for loss separation including the currents, the electrical parameters of the machine and the recorded winding temperatures.

loss induced by friction in the ball bearings and the iron losses in the laminated stator and the rotor iron, respectively. Assuming that the motor is symmetrical,  $R_{uv} = R_{vw} = R_{wu}$  and  $I_s = I_u = I_v = I_w$ , the Joule losses can be estimated by

$$P_{js} = \frac{3I_s^2}{2} R_{t,20} (1 + \alpha_{cu,20} (\bar{T}_w - 20^\circ\text{C})), \quad (2)$$

where  $I_s$  is the effective current measured by a power analyzer,  $R_{t,20}$  is the terminal resistance at  $20^\circ\text{C}$  from Table I,  $\alpha_{cu,20}$  is the linear temperature coefficient of copper at  $20^\circ\text{C}$ , and  $\bar{T}_w$  is the averaged winding temperature as shown in Fig. 5. Hence, the residual losses are given by  $P_{\text{residual}} = P_{\text{loss}} - P_{js}$ . The subdivision of residual losses into the remaining power sources  $P_{Fe}$  and  $P_{rot}$  is very complex and generally depends on the current load point. However, for this analysis and to minimize the number of parameters to be optimized, a constant loss ratio  $P_{rot} = k_{p,rot} P_{\text{residual}}$  and  $P_{Fe} = (1 - k_{p,rot}) P_{\text{residual}}$ , with the dimensionless parameter  $k_{p,rot} = 0.1$  is chosen for now.

### B. Speed dependent thermal resistances

All parameters analytically calculated in Section III are derived on basic and simplified theories, e.g., the hollow cylinder theory and convection on static cylinders and plates. However, measurements presented in Section IV show speed-dependent heating and cooling effects that cannot be explained by this simplified modeling approaches. Hence, the speed-dependent behavior should be calibrated by using an optimization algorithm. In this analysis a linear speed dependency for a thermal resistance

$$R_i(n) = R_{i,0} \left( 1 - \frac{|n|}{n_{\max}} (1 - k_{i,s}) \right) + \Delta R_{i,0} \delta(n), \quad (3)$$

where  $n$  is the rotational speed of the rotor bell,  $R_{i,0} = R_i(0)$  is the additive thermal resistance value at zero speed,  $n_{\max} = 7500$  rpm is the maximal reachable speed of the bell,  $k_{i,s}$  is the parameter to be optimized, and  $\delta(n)$  is the delta-distribution, is assumed. In the following optimization the air gap and the heat flow from rotor to ambient are modeled as speed-dependent, i.d.  $i = \{\text{ra, airgap}\}$ . The function is illustrated in Fig. 6. For this approach, only two parameters are required to be estimated, which keep the total parameter count reasonable, but it is able to represent both the high thermal resistance at standstill due to natural convection, as well as the decrease of thermal resistance because of forced convection at higher speeds.

### C. Applied optimizing technique

In summary, the uncertain parameters to be estimated are  $R_{ra,0}$ ,  $R_{airgap,0}$ ,  $R_{sa}$ ,  $R_{ig}$ ,  $k_{ra,s}$ ,  $k_{airgap,s}$ ,  $\Delta R_{ra,0}$ ,  $\Delta R_{airgap,0}$ , and  $\Delta R_{sa,0}$ . Thanks to the analytical approximations, a limitation of the design space is possible, but nevertheless the considered domain is high-dimensional. In order to find the global minimum and the corresponding best parameter setting, a genetic algorithm (GA) from the Java-based multi-objective optimization framework jmetal is used [22]. This type of algorithm is inspired by evolutionary principles from

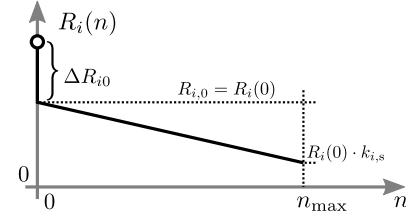


Fig. 6: Proposed function of a thermal resistance  $R_i(n)$  depending on the speed of the rotor bell  $n$ .

Parameter at 20 °C	Initial value	Optimized value
$R_{\text{theet}}$	$0.24 \text{ K W}^{-1}$	
$R_{sy1}$	$0.024 \text{ K W}^{-1}$	
$R_{sy2}$	$0.028 \text{ K W}^{-1}$	
$R_{ig}$	$1.00 \text{ K W}^{-1}$	$1.34 \text{ K W}^{-1}$
$R_{cu}$	$2.75 \text{ K W}^{-1}$	
$R_{airgap,0}$	$11.3 \text{ K W}^{-1}$	$4.11 \text{ K W}^{-1}$
$R_{ra,0}$	$1.74 \text{ K W}^{-1}$	$2.28 \text{ K W}^{-1}$
$R_{sa}$	$1.20 \text{ K W}^{-1}$	$3.79 \text{ K W}^{-1}$
$C_{\text{rot}}$	$122 \text{ J K}^{-1}$	
$C_{\text{theet}}$	$31.4 \text{ J K}^{-1}$	
$C_{ys}$	$27.7 \text{ J K}^{-1}$	
$C_{\text{sfix}}$	$125 \text{ J K}^{-1}$	
$C_{cu}$	$19.8 \text{ J K}^{-1}$	
$k_{ra,s}$	1.0	0.13
$k_{airgap,s}$	1.0	0.18
$\Delta R_{ra,0}$	$0.0 \text{ K W}^{-1}$	$3.43 \text{ K W}^{-1}$
$\Delta R_{airgap,0}$	$0.0 \text{ K W}^{-1}$	$1.25 \text{ K W}^{-1}$
$\Delta R_{sa,0}$	$0.0 \text{ K W}^{-1}$	$14.1 \text{ K W}^{-1}$

TABLE III: Comparison of the analytically determined and the optimized parameter set

nature and can facilitate solve highly non-linear and multi-dimensional problems [23]. Furthermore, the difficulty of selecting a sufficient starting set of parameters is solved by using a latin hypercube sampling (LHS) based approach. It generates an initial set of parameter combinations fairly distributed within the design space. A suitable cost function

$$c = \sqrt{\sum_{m=1}^M \frac{1}{N} \sum_{s=1}^N (T_{j,\text{mod}}[s] - T_{j,\text{meas}}[s])^2} \quad (4)$$

has been applied, where  $T_{j,\text{mod}}[s]$  is the  $j$ -th temperature calculated by the model at time  $s$ ,  $T_{j,\text{meas}}[s]$  is the  $j$ -th temperature measured using experimental setup at the same time,  $N$  is the total number of samples, and  $M$  is the total number of considered temperatures within the optimization. This definition of the cost value can be interpreted as an averaged effective temperature error between calculated and measured temperatures. Table III compares the initial values found by analytical approaches and the optimal parameters estimated by a LHS followed by running the GA.

#### D. Optimization results

The LHS is used to randomly generate 4000 design variants before the GA is applied to minimize the cost functional (4), where at most 4000 thermal models are calculated by using a population size of 50 individuals. The presented optimization requires approximately 60 h on a single computer that uses four processor cores with 3.42 GHz clock frequency.

Figures 7 and 8 show the measured temperature curves used for optimization. They are a combination of two different measurement runs, a static one with eight different load points and a dynamic load profile with 49 load steps. If the initial values are used without any adjustment, the cost function value is  $c_{\text{initial}} = 9.93 \text{ }^{\circ}\text{C}$ .

According to Fig. 7, the initial network can model the dynamic variation of load points with high accuracy. As shown in the second diagram of Fig. 7, the residual of the

temperatures varies in a range of  $0 \text{ }^{\circ}\text{C}$  and  $-8 \text{ }^{\circ}\text{C}$ . Hence, the estimated heat capacities from Table III describe the thermal behavior of the motor well. In contrast, the estimation of the static thermal behavior exhibits higher errors, e.g., up to  $13 \text{ }^{\circ}\text{C}$  for the winding temperature. Hence, the estimated values of the thermal resistances, which mainly determine the static performance of the network, are supposed to feature significant modeling errors.

As presented in Fig. 8, the thermal network with optimized parameters models the static and the dynamic behavior of the motor more accurately. For this reason, the value of cost function is reduced to  $c_{\text{opt}} = 2.28 \text{ }^{\circ}\text{C}$ , which is more than four times smaller compared to the initial setting. Additionally, the maximum error for both load variations is always within  $\pm 5 \text{ }^{\circ}\text{C}$ , and most of the time even smaller than  $\pm 2.5 \text{ }^{\circ}\text{C}$ .

The modeling error is larger at higher temperatures, e.g. for

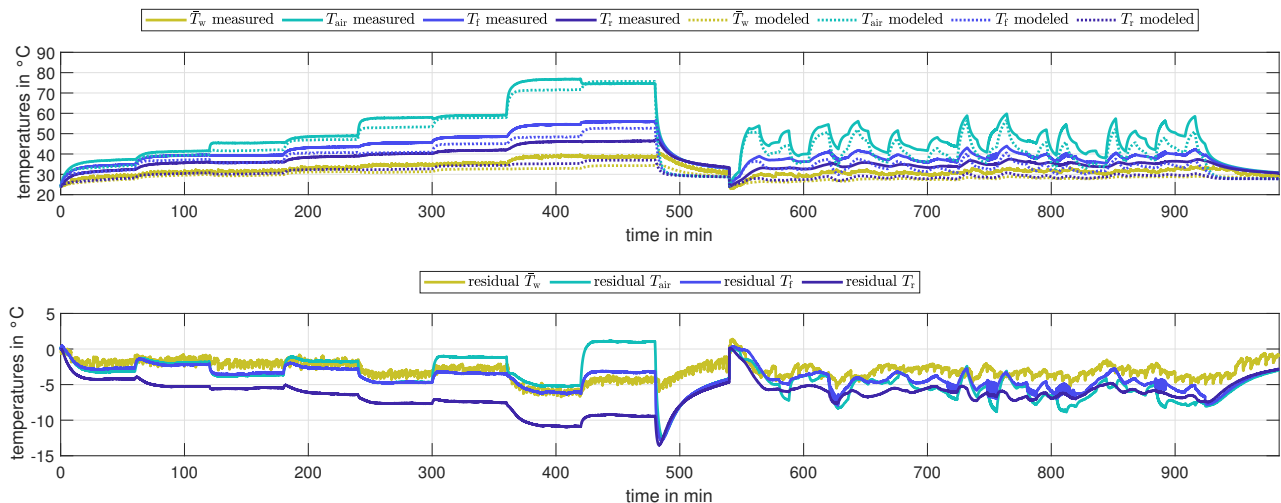


Fig. 7: Comparison of the measured temperature curves with those calculated by the thermal model using the initial parameter set determined by analytical approaches in Section III.

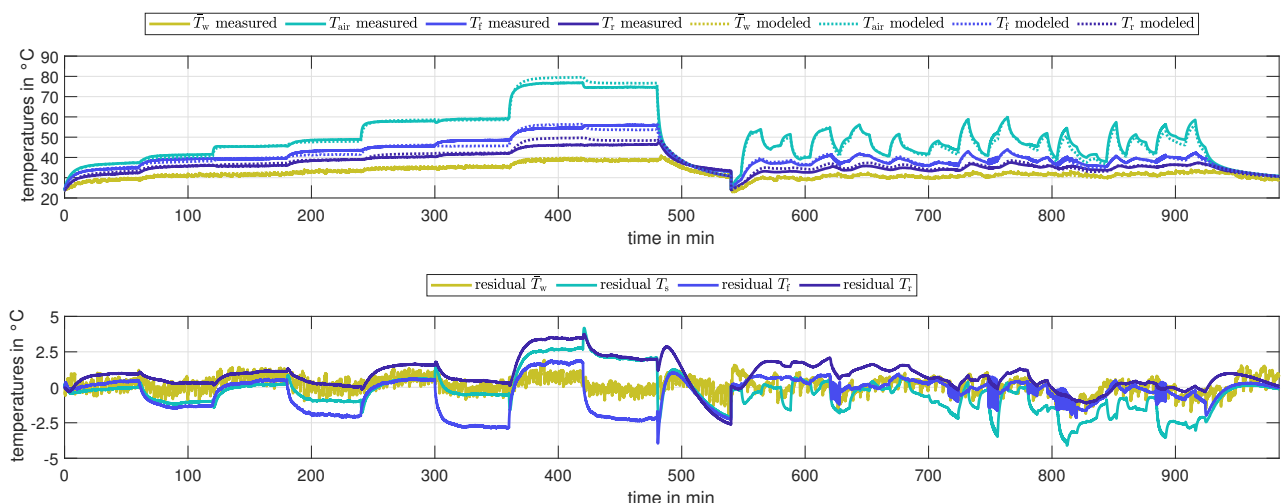


Fig. 8: Comparison of the measured temperature curves with those calculated by the thermal model using the optimized parameter set derived in Section V.

the winding temperature between the points in time 360 min and 420 min, because of the limited data available within this temperature range. Consequently, such load points are under-represented in the optimization scenario.

The initial network cannot correctly predict the high speed characteristics of the motor, as shown in the time range between 420 min and 480 min. The winding temperature decreases despite higher load torque due to the high speed. In contrast, the optimized model with a speed-dependent thermal resistance is able to consider this circumstance more accurate. Additionally, the modeling of the cooling phases when the motor is stopped are significantly improved.

## VI. CONCLUSION

This paper gives an overview about measurement-based optimization of a thermal model for an outer rotor PM machine. First, an initial physics-based thermal network with thermal resistances and heat capacities is introduced. Based on these analytical approaches, the initial parameters of the network are determined or, in the case of convective heat transfer, roughly estimated. Consequently, the uncertain parameters are identified by using a genetic algorithm with a latin hypercube sampling-based start-up. Additionally, a loss separation and a speed-dependent modeling of convective heat transitions are introduced. Finally, the mean effective temperature error is reduced by a factor of 4.3. In future works, the aim is to further improve the modeling precision by making the loss separation parameter  $k_{p,\text{rot}}$  speed- and temperature-dependent.

## ACKNOWLEDGMENT

This work has been supported by the COMET-K2 “Center for Symbiotic Mechatronics” of the Linz Center of Mechatronics (LCM) funded by the Austrian federal government and the federal state of Upper Austria. The authors thank ebmpapst St. Georgen GmbH & Co. KG, the manufacturer of the motor under test, who provided the machine for this study.

## REFERENCES

- [1] B. Fahimi, O. Mohammed, H. Toliyat, J. Kirtley, S. Pekarek, L. Parsa, K. Hameyer, A. Sarikhani, E. Muljadi, and J. Hendershot, “Guest Editorial Optimal Design of Electric Machines,” *IEEE Transactions on Energy Conversion*, vol. 30, no. 3, pp. 1143–1143, sep 2015. [Online]. Available: <http://ieeexplore.ieee.org/document/7208745/>
- [2] G. Bramerdorfer, J. A. Tapia, J. J. Pyrhönen, and A. Cavagnino, “Modern Electrical Machine Design Optimization: Techniques, Trends, and Best Practices,” *IEEE Transactions on Industrial Electronics*, vol. 65, no. 10, pp. 7672–7684, 2018.
- [3] A. Cavagnino, G. Bramerdorfer, and J. A. Tapia, “Optimization of electric machine Designs - Part I,” *IEEE Transactions on Industrial Electronics*, vol. 64, no. 12, pp. 9716 – 9720, 2017.
- [4] ——, “Optimization of Electric Machine Designs - Part II,” *IEEE Transactions on Industrial Electronics*, vol. 65, no. 2, pp. 1700–1703, 2017.
- [5] A. Fatemi, D. M. Ionel, M. Popescu, Y. C. Chong, and N. A. O. Demerdash, “Design Optimization of a High Torque Density Spoke-Type PM Motor for a Formula E Race Drive Cycle,” *IEEE Transactions on Industry Applications*, vol. 54, no. 5, pp. 4343–4354, sep 2018. [Online]. Available: <https://ieeexplore.ieee.org/document/8374899/>
- [6] M. Popescu, I. Foley, D. A. Staton, and J. E. Goss, “Multi-physics analysis of a high torque density motor for electric racing cars,” *2015 IEEE Energy Conversion Congress and Exposition, ECCE 2015*, no. September, pp. 6537–6544, 2015.
- [7] G. Lei, T. Wang, J. Zhu, Y. Guo, and S. Wang, “System-Level Design Optimization Method for Electrical Drive Systems—Robust Approach,” *IEEE Transactions on Industrial Electronics*, vol. 62, no. 8, pp. 4702–4713, aug 2015. [Online]. Available: <http://ieeexplore.ieee.org/document/7042818/>
- [8] B. Assaad, K. El Kadri Benkara, G. Friedrich, S. Vivier, and A. Michon, “Reducing the complexity of thermal models for electric machines via sensitivity analyses,” *2017 IEEE Energy Conversion Congress and Exposition, ECCE 2017*, vol. 2017-Janua, pp. 4658–4665, 2017.
- [9] D. A. Staton and A. Cavagnino, “Convection heat transfer and flow calculations suitable for electric machines thermal models,” *IEEE Transactions on Industrial Electronics*, 2008.
- [10] A. Boglietti, A. Cavagnino, M. Lazzari, and M. Pastorelli, “A Simplified Thermal Model for Variable-Speed Self-Cooled Industrial Induction Motor,” *IEEE Transactions on Industry Applications*, 2003.
- [11] P. Giangrande, V. Madonna, S. Nuzzo, C. Spagnolo, C. Gerada, and M. Galea, “Reduced order lumped parameter thermal network for dual three-phase permanent magnet machines,” *Proceedings - 2019 IEEE Workshop on Electrical Machines Design, Control and Diagnosis, WEMDCD 2019*, vol. 1, pp. 71–76, 2019.
- [12] M. Popescu, D. A. Staton, A. Boglietti, A. Cavagnino, D. Hawkins, and J. Goss, “Modern Heat Extraction Systems for Power Traction Machines - A Review,” *IEEE Transactions on Industry Applications*, 2016.
- [13] F. Boseniuk and B. Ponick, “Parameterization of transient thermal models for permanent magnet synchronous machines exclusively based on measurements,” *2014 International Symposium on Power Electronics, Electrical Drives, Automation and Motion, SPEEDAM 2014*, pp. 295–301, 2014.
- [14] L. Ma, L. Zhao, and X. Wang, “Prediction of thermal system parameters based on PSO-ELM hybrid algorithm,” *Proceedings - 2017 Chinese Automation Congress, CAC 2017*, vol. 2017-Janua, pp. 3136–3141, 2017.
- [15] W. Kirchgassner, O. Wallscheid, and J. Böcker, “Deep residual convolutional and recurrent neural networks for temperature estimation in permanent magnet synchronous motors,” *2019 IEEE International Electric Machines and Drives Conference, IEMDC 2019*, pp. 1439–1446, 2019.
- [16] Z. Xu, Y. Gao, X. Wang, X. Tao, and Q. Xu, “Surrogate Thermal Model for Power Electronic Modules using Artificial Neural Network,” in *IECON 2019 - 45th Annual Conference of the IEEE Industrial Electronics Society*, vol. 1. IEEE, oct 2019, pp. 3160–3165. [Online]. Available: <https://ieeexplore.ieee.org/document/8927494/>
- [17] K. Zhang, A. Guliani, S. Ogreni-Memik, G. Memik, K. Yoshii, R. Sankaran, and P. Beckman, “Machine Learning-Based Temperature Prediction for Runtime Thermal Management Across System Components,” *IEEE Transactions on Parallel and Distributed Systems*, vol. 29, no. 2, pp. 405–419, 2018.
- [18] G. Guedia Guemo, P. Chantrenne, and J. Jac, “Parameter identification of a lumped parameter thermal model for a permanent magnet synchronous machine,” *Proceedings of the 2013 IEEE International Electric Machines and Drives Conference, IEMDC 2013*, pp. 1316–1320, 2013.
- [19] C. Sciascera, P. Giangrande, L. Papini, C. Gerada, and M. Galea, “Analytical Thermal Model for Fast Stator Winding Temperature Prediction,” *IEEE Transactions on Industrial Electronics*, vol. 64, no. 8, pp. 6116–6126, aug 2017. [Online]. Available: <http://ieeexplore.ieee.org/document/7878526/>
- [20] D. Staton, A. Boglietti, and A. Cavagnino, “Solving the More Difficult Aspects of Electric Motor Thermal Analysis in Small and Medium Size Industrial Induction Motors,” *IEEE Transactions on Energy Conversion*, vol. 20, no. 3, pp. 620–628, sep 2005. [Online]. Available: <http://ieeexplore.ieee.org/document/1495534/>
- [21] A. Boglietti, M. Cossale, S. Vaschetto, and T. Dutra, “Thermal Conductivity Evaluation of Fractional-Slot Concentrated-Winding Machines,” *IEEE Transactions on Industry Applications*, vol. 53, no. 3, pp. 2059–2065, 2017.
- [22] J. J. Durillo and A. J. Nebro, “jmetal: A java framework for multi-objective optimization,” *Advances in Engineering Software*, vol. 42, pp. 760–771, 2011. [Online]. Available: <http://www.sciencedirect.com/science/article/pii/S0965997811001219>
- [23] M. Mitchell, *An Introduction to Genetic Algorithms*. Cambridge, MA, USA: MIT Press, 1996.